



HAL
open science

Influence of wire feed speed and torch speed on the mechanical properties of wire arc additively manufactured stainless steel

Laurent Terrenoir, Julie Lartigau, Arun Arjunan, Laura Laguna Salvadó,
Christophe Merlo

► To cite this version:

Laurent Terrenoir, Julie Lartigau, Arun Arjunan, Laura Laguna Salvadó, Christophe Merlo. Influence of wire feed speed and torch speed on the mechanical properties of wire arc additively manufactured stainless steel. Journal of Manufacturing Science and Engineering, In press, pp.1-44. <10.1115/1.4063108>. <hal-04185329>

HAL Id: hal-04185329

<https://hal.science/hal-04185329v1>

Submitted on 9 Jan 2026

HAL is a multi-disciplinary open access archive for the deposit and dissemination of scientific research documents, whether they are published or not. The documents may come from teaching and research institutions in France or abroad, or from public or private research centers.

L'archive ouverte pluridisciplinaire **HAL**, est destinée au dépôt et à la diffusion de documents scientifiques de niveau recherche, publiés ou non, émanant des établissements d'enseignement et de recherche français ou étrangers, des laboratoires publics ou privés.



HAL Authorization



Laurent Terrenoir¹

ESTIA Institute of Technology,
University of Bordeaux,
F-64210 Bidart, France
e-mail: l.terrenoir@estia.fr

Julie Lartigau

ESTIA Institute of Technology,
University of Bordeaux,
F-64210 Bidart, France
e-mail: j.lartigau@estia.fr

Arun Arjunan

Additive Manufacturing of Functional Materials
Research Group (AMFM),
School of Engineering, Computing and
Mathematical Sciences,
University of Wolverhampton,
Telford Campus,
Wolverhampton TF2 9NT, UK
e-mail: a.arjunan@wlv.ac.uk

Laura Laguna Salvado

ESTIA Institute of Technology,
University of Bordeaux,
F-64210 Bidart, France
e-mail: l.lagunasalvado@estia.fr

Christophe Merlo

ESTIA Institute of Technology,
University of Bordeaux,
F-64210 Bidart, France
e-mail: c.merlo@estia.fr

Influence of Wire Feed Speed and Torch Speed on the Mechanical Properties of Wire Arc Additively Manufactured Stainless Steel

Wire arc additive manufacturing (WAAM) enables 3D printing of large high-value metal components. However, integrating WAAM into production lines requires a critical understanding of the influence of process parameters on the resulting material characteristics. As such, this research investigates the relationship between WAAM wire feed speed (WFS) and torch speed (TS) on the resulting mechanical characteristics of 316LSi thick parts (2.5 cm (0.98 in.)). The experimental procedure is informed by a training matrix that allows parametric analysis of WFS and TS on the ultimate tensile strength (σ_{ult}), yield strength (σ_y), elastic modulus (E), failure strain (ϵ_f), hardness (HV0.5), and dimensional accuracy (D_a) of the printed samples. The research found that WAAM-processed 316LSi parts feature isotropic material properties despite variations in WFS and TS. The surrogate model developed in this study offers five significant polynomial models capable of accurately predicting the influence of WAAM process parameters on σ_{ult} , σ_y , ϵ_f , E , and D_a . The research found TS to be the most significant WAAM process parameter in comparison to WFS for σ_{ult} and ϵ_f . On the contrary, σ_y , E , and D_a were found to be primarily driven by WFS as opposed to TS. Overall, the paper for the first time presents an accurate surrogate model to predict the mechanical characteristics of WAAM 316LSi thick parts informed by wire feed speed and torch speed. The study demonstrates that the mechanical properties of WAAM-processed steel are primarily influenced by the underlying process parameters offering significant potential for tunable performance. [DOI: 10.1115/1.4063108]

Keywords: additive manufacturing, modeling and simulation, process engineering

1 Introduction

Wire arc additive manufacturing (WAAM) has proven to be a highly effective technique in the metal AM field due to its low material wastage and high deposition rate [1–3]. This method involves melting a metal wire through an electric arc, which deposits the material in a layer-by-layer fashion [4]. Ongoing research efforts have focused on addressing challenges such as in situ monitoring of WAAM [5] and the development and characterization of novel metallic materials [6,7]. To lower the heat input during the WAAM process, Fronius International GmbH has developed the cold metal transfer (CMT) variant of WAAM. This variant manages the energy of the electric arc and wire retraction through a push-and-pull electromechanical process during deposition [8].

As a result, WAAM CMT is an improved process [9] suitable to manufacture large high-value metal components suitable for a range of industries [2]. Literature [10,11] so far on WAAM processes highlights the importance of controlling the energy input as the primary influencer on the thermal history of the manufactured

part dictating its mechanical properties. However, as suggested by Rodrigues et al. [8], further refinement in the process knowledge is necessary to optimize WAAM process parameters to predict bulk material properties for industrial application which this research aims to contribute.

Although research on WAAM has been primarily targeted at aluminum (Al) and titanium (Ti) due to their increasing application for light weighting and specialists applications [8,12–15], some recent work focused on steel as it is still the most widely used metal when it comes to the industry as a whole [16–18]. WAAM of 316LSi stainless steel is of significant interest due to its use in large structural parts suitable for industries such as construction, defence, energy, naval, and tooling [2,8,15]. It has also been found suitable for functionally graded materials [19]. Studies on WAAM of 316LSi reveal that suboptimal process parameter leads to inferior mechanical performances and geometrical accuracy primarily dictated by excessive heat accumulation [20]. Although WAAM is faster in comparison to other AM processes, it offers inferior geometrical accuracy. Nowadays, process parameters are chosen accordingly to printability and to meet mechanical requirements, as stated by Evans et al. [21].

Numerous studies [22–27] have been conducted in this regard on a range of materials to identify process parameters for the precise

¹Corresponding author.

Manuscript received March 15, 2023; final manuscript received August 1, 2023; published online August 28, 2023. Assoc. Editor: Vincent Wagner.

control of bead height and width. When it comes to single beads, their thickness and deposition rate are informed by a range of process and material parameters which include the energy input (e_t), wire feed speed (WFS), wire thickness, and torch speed (TS). When it comes to steel, wire diameters of 0.8–1.2 mm (0.18–0.28 picas) are often used, accordingly to the wire feeding system, leading to a thickness in the range of 3.5–8 mm (0.83–1.89 picas) for an individual bead [28–30]. Although studies have explored the influence of WAAM process parameters on single and multiple beads in isolation, the observations do not always translate to improving the quality of thick parts. Although limited, some studies on WAAM 316LSi have characterized the isotropy of the tensile properties and the hardness variation under varying process parameters [20,31]. Nevertheless, studies focused on exposing the optimum WAAM process parameters suitable for thick (25 mm (0.98 in.)) steel parts offering high structural integrity are yet to be carried out.

The latest literature on the mechanical behavior of WAAM of steel explores its hardness and tensile properties. There are certain cases where WAAM has offered mechanical properties similar to that of conventionally manufactured parts [32], this is not always the case [28]. It appears to be due to the geometry of the part and the process parameters which influences the metallurgical phases through heat input and cooling [33]. Meaning, an in-depth analysis of the relationship linking the process parameters and the mechanical behavior of WAAM is called for [15]. Research carried out by Wang et al. [31] showed that the energy input during the WAAM process impacts both the microstructure and the bulk properties of the fabricated parts. This is of particular interest when studying WAAM process parameters as the energy input can vary significantly despite using a constant wire feed speed [31]. For instance, with the same process parameters and varying only the heat input, from 260 to 470 J/mm, Cunningham et al. [28] found variations in elasticity modulus (from 165 GPa to 141 GPa) and ultimate tensile strength (from 579 MPa to 565 MPa). But when it comes to estimating this impact, there is no existing analytical model, such as equations linking the tensile properties or hardness of a part to the first-order process parameters. Another phenomenon of interest is the metal transfer mode which influences the resulting mechanical properties of produced parts [34–36].

Despite the success of WAAM of steel, Jin et al. [37] in their review reveal that there is still a lack of a holistic view on this topic. Overall, the bulk performance of the fabricated material is closely related to wire and torch speed, heat input, cooling time, and interlayer temperature. Although there is significant interest, no comprehensive model of the impact of process parameters on the geometrical accuracy, tensile properties, and hardness of thick WAAM 316LSi stainless steel are reported [38,39]. To address this gap, the research conceives the question: How do the WAAM process parameters affect the mechanical properties of thick 316L steel? To answer this question, the research investigates

the use of WAAM to fabricate 25 mm thick 316L stainless steel samples. Nine different combinations of process parameters informed by a range of wire and torch speeds were studied. The print quality of the samples was analyzed using 3D scanning technology to characterize the influence of WAAM on the dimensional accuracy of the prints. Subsequently, tensile and hardness tests were carried out to reveal the mechanical behavior of the samples. The physical test data were also used to develop a surrogate model capable of predicting the mechanical performance of WAAM stainless steel. The study also introduces a response surface model capable of characterizing the interaction effects of the process parameter wire (WFS) and TS on elastic modulus (E), yield strength (σ_y), ultimate tensile strength (σ_{ult}), fracture strain (ϵ_f), and the dimensional accuracy (D_a). The hardness (HV0.5) for the printed samples were also characterized and found to be not in direct co-relation with WFS and TS. This is the first research to bring forward a surrogate model that links the WAAM wire and torch speed to the mechanical properties of 316LSi steel for decision making.

2 Materials and Methods

2.1 Manufacturing Process. The fabrication of all the samples evaluated in this study was carried out using the FRONIUS TransPuls Synergic 3200 CMT WAAM station coupled to a robot KUKA KR 100 HA 2000. Communications between the robot and the WAAM system were enabled through the AB Device Net protocol. The chosen feedstock was a 316LSi stainless steel wire of diameter 1.2 mm (0.28 pica) whose composition is given as G 19 12 3 L Si, following ISO 14,343-A standard [40]. The samples were additively manufactured on a 316L stainless steel plate of dimension 300 × 120 × 18 mm (11.8 × 4.7 × 0.7 in.). The welding torch was mounted on the robotic arm from which the wire was fed as shown in Fig. 1(a). The material was deposited layer-by-layer on the substrate following a bidirectional triangular scanning path. All first-order and second-order process parameters are detailed in the next section. A pyrometer was used to monitor the interlayer temperature set at 400 °C (752 °F) during the manufacturing process. In practice, the interlayer time is equal to the cooling time of the upper layer to 400 °C. The temperature was measured in the middle of the upper layer. Once the measured temperature underreached 400 °C, the pyrometer was relocated to target the next layer and the fabrication was restarted.

2.2 Process Parameters. For WAAM, the thermal history and thus the deposited material properties are dictated by the heat input (e_t) in J/mm [41,42] which is calculated as follows:

$$e_t = \eta \times \frac{U \times I}{TS} \quad (1)$$

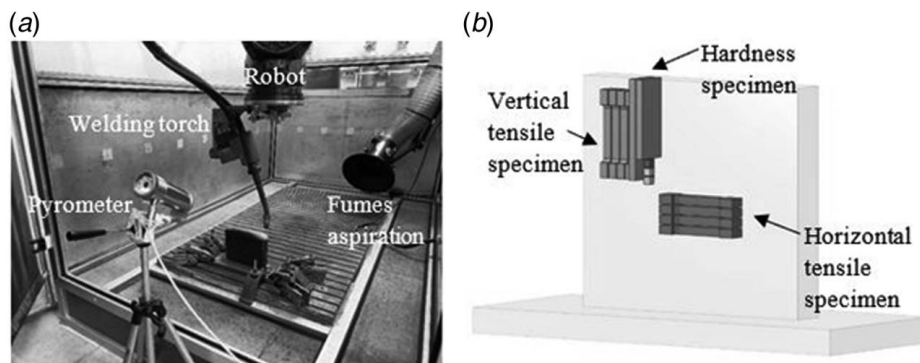


Fig. 1 Wire arc additive manufacturing facility showing (a) the fabrication setup used and (b) the build orientation for sample extraction

Table 1 Nominal first-order process parameters WFS and TS and the related nominal second-order process parameters

Part reference	WFS (m/min)	TS (m/min)	U (V)	I (A)	e_i (J/mm)	Scanning period (mm)
(a)	5	0.60	12.5	165	165	3.6
(b)	7.5	0.60	13.4	219	234	5.2
(c)	10	0.60	14.0	260	291	6.0
(d)	5	0.75	12.5	165	132	3.2
(e)	7.5	0.75	13.4	219	188	4.5
(f)	10	0.75	14.0	260	233	5.4
(g)	5	0.90	12.5	165	110	2.9
(h)	7.5	0.90	13.4	219	157	4.1
(i)	10	0.90	14.0	260	194	4.3

where η is the energy efficiency. For WAAM CMT, it is 80% [43,44]. U is the welding voltage in V, and I is the welding current, in A, responsible for the creation of the electric arc. U and I are linked to WFS which is the wire feed speed, i.e., the speed at which the wire (feedstock) goes through the welding torch. Through the synergic laws developed by Fronius, U and I are determined according to WFS. TS is the torch speed, expressed in mm/s. TS is the speed of displacement of the robot holding the welding torch through the scanning path. There are numerous considerations when determining the limits of the process parameters to inform the training matrix. The first one is that the chosen parametric combinations should achieve a consistent, fully dense track. Generally, both the wire and torch speed are carefully controlled to ensure the right amount of heat input. Insufficient heat input causes incomplete layers melting which is one of the factors leading to the formation of porosity [45]. On the contrary, high heat input might lead to an unstable melt pool and poor geometrical accuracy, depending on the geometry of the printed part and the deposition strategy [46]. As such, there is an optimum parametric window that achieves a continuously fused material track [47].

The first-order WAAM process parameters are WFS and TS. Second-order process parameters such as current, voltage, heat input, and the scanning period of the triangular deposit vary according to the chosen values of WFS and TS. The nominal values for these varying process parameters are summarized in Table 1.

The mean measured values for WFS current, voltage, and mean layers height are displayed in Table 2. The estimated heat input based on the measured values of current and intensity is also provided. The fixed second-order parameters are synthesized in Table 3.

2.3 Post-Processing. A heat treatment was applied to all produced parts (4 h at 500 °C (932 °F) with heating and cooling phases of 50 °C/h (122 °F/h) to remove the residual stresses without significantly modifying the mechanical properties of the printed material. Following the heat treatment, the parts were post-processed using five-axis and electrical discharge machining

(EDM) to extract the test samples which are mentioned in Table 4. Regarding tensile specimens, two sample orientations (vertical and horizontal) as shown in Fig. 1(b) were considered to check the isotropy of the fabricated material. For each direction, three specimens were cut out for each part. Regarding the hardness specimens, all the tests were carried out on polished flat samples that were extracted using submerged wire EDM.

2.4 Characterization of Dimensional Accuracy. Among the range of additive manufacturing technologies, WAAM is commonly acknowledged as the most appropriate method for producing sizeable components. Small dimensional inaccuracies during printing can become significant changes when translated to large parts affecting the limits and fits. As such the dimensional accuracy becomes a significant parameter when characterizing the quality of WAAM parts. In this study, the dimensional accuracy parameter estimates the discrepancies between the surfaces of each printed sample and their ideal computer-aided design (CAD) [48]. On Figs. 2(a) and 2(b), an exaggerated representation of the difference between a printed sample and the targeted CAD is schematized.

To evaluate the accuracy between the surface of the manufactured part and the targeted CAD, the distance between each pairwise points ϵ_{ij} of both surfaces (printed and targeted) is measured all over the additively manufactured part.

Then for each part, the mean distance between all points of the surface of the printed sample and the targeted geometry is calculated. The mean ($D_{a(\text{mean})}$) and maximum ($D_{a(\text{max})}$) distance between each pairwise points of the surface of the manufactured part and the surface of the targeted part (the CAD) were measured, as informed by the literature [49,50]. They are defined by Eqs. (2) and (3).

$$D_{a(\text{mean})} = \frac{\sum_{j=1}^n \sum_{i=1}^m \epsilon_{ij}}{i \times j} \quad (2)$$

$$D_{a(\text{max})} = \max(\epsilon_{ij}) \quad (3)$$

Table 2 Measured WFS and specific second-order process parameters

Part ref	Measured parameters					Calculated parameters e_i (J/mm)
	WFS (mean) (m/min)	U (mean) (V)	I (mean) (A)	Number of layers	Layers height (mean) (mm)	
(a)	5.6 ± 0.6	11.9 ± 0.8	159.2 ± 5.5	31	5.2 ± 0.6	151.6 ± 11.5
(b)	8.0 ± 1.3	13.4 ± 1.5	205.8 ± 8.7	35	4.7 ± 0.3	220.6 ± 26.4
(c)	9.7 ± -1.7	15.9 ± 1.6	218.5 ± -14.6	38	4.3 ± 0.6	277.9 ± 28.6
(d)	5.3 ± -0.5	11.5 ± 0.6	159.8 ± 2.3	34	4.8 ± 0.6	117.6 ± 6.4
(e)	8.3 ± -1.4	13.7 ± 1.5	209.5 ± 8.5	37	4.4 ± 0.7	183.7 ± 21.4
(f)	9.2 ± -1.3	14.0 ± 1.5	229.1 ± 15.7	46	3.5 ± 1	205.3 ± 22.6
(g)	5.2 ± -0.6	11.6 ± 0.6	158.7 ± 4.8	35	4.7 ± 0.5	98.2 ± 5.9
(h)	7.8 ± -0.9	13.2 ± 0.9	210.3 ± 8.4	38	4.3 ± 0.8	148.1 ± 11.7
(i)	8.7 ± -1.3	14.9 ± 1.3	226.4 ± 14.5	40	4.0 ± 0.6	179.9 ± 16.1

Table 3 Synthesis of deposit and WAAM second-order process parameters used

Deposit	Height/width/length	160 mm × 25 mm × 180 mm
	Deposition strategy	Triangular path—bidirectional
	Scanning amplitude	25 mm
WAAM process	Shielding gas	Mison 2 (Ar + 2% CO ₂ + 0.03% NO)
	Shielding gas rate	17 L/min
	CMT synergic law	CMT 1627—base 0979
	Stick out	15 mm
Interlayer temperature		400 °C

The dimensional accuracy (D_a) is defined as $D_{a(\text{mean})}$ scaled down to a percentage of the part's dimensions, in this case its targeted height (H_t), as described by Eq. (4). The targeted height (H_t), represented in Fig. 2(a), is 160 mm (6.3 in.).

$$D_a = 1 - \frac{D_{a(\text{mean})}}{H_t} \quad (4)$$

To characterize the dimensional accuracy, the printed samples were scanned using the Faro robot laser scanning arm featuring

non-contact laser line probe technology, where the laser is informed by the FARO CAM2 software. The scanned samples were compared with the ideal geometry informed by the original CAD.

2.5 Tensile Testing. To analyze the stress–strain (σ – ϵ) behavior of WAAM 316LSi stainless steel, 54 test specimens were subjected to tensile testing. The configuration of the tensile specimens taken from the printed part are presented in Table 4. The tensile tests were performed using a Zwick Roell Z1474 universal material testing machine that has a maximum load capacity of 100 kN. Prior to conducting the experiments, the equipment was calibrated and validated in accordance with BSENISO 7500-1 (O 7500-1:2018—Metalli, 2018). To ensure quasi-static deformation as specified by the ISO 6892-1:2019(E) [51] standard, the test coupons were pulled to failure at a rate of 0.63 mm/min. Deformation beyond the elastic limit was necessary to analyze the failure modes and the overall behavior of the material processed by WAAM. To capture the fine strain around the yield zone, a five-millimeter gauge extensometer, as shown in Fig. 3, was affixed to each of the samples. Based on the σ – ϵ curve, the properties of the test samples were characterized for elastic modulus (E), fracture strain (ϵ_f), yield strength (σ_y), and ultimate strength (σ_{ult}). To

Table 4 Shape, size, and number (n) of extracted specimens from WAAM 316LSi samples for mechanical testing

Type	Shape and size	Specimen count (n)
Horizontal tensile specimen		3 per parts $n = 27$
Vertical tensile specimen		3 per part $n = 27$
Hardness specimen		1 per part $n = 9$ Number of indentations: $N_i = 9 \times 15 = 135$

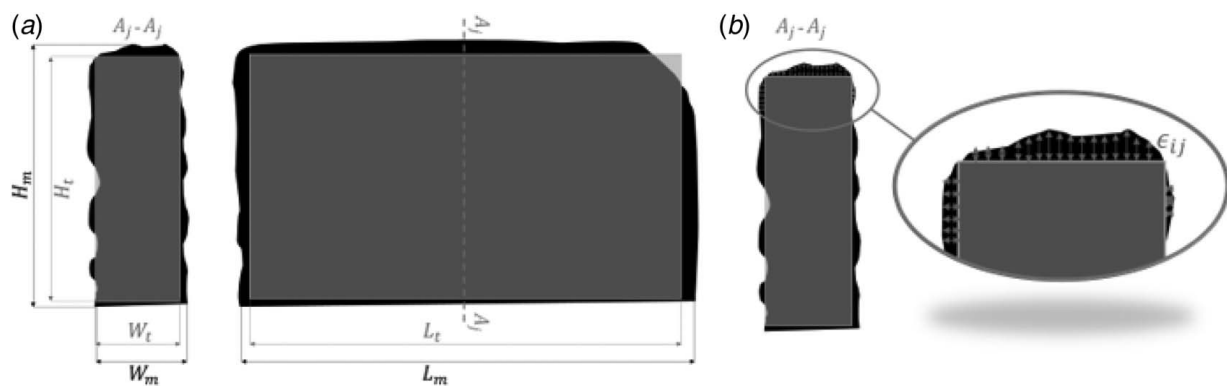


Fig. 2 Schematic representation of the difference between the surfaces of the printed part (in black) and the targeted geometry (in grey) (a) in general view and (b) cross-sectional view

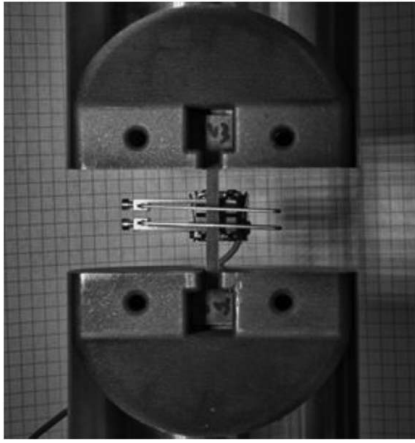


Fig. 3 Mechanical testing of the WAAM samples showing the non-slipping platens and the placement of the fine strain extensometer mounted to the test specimen

avoid data contamination due to sample slippage, non-slip platens were utilized for all mechanical testing.

2.6 Hardness Testing. The Vickers hardness tests were carried out using a Zwick/Rowell Indentec hardness machine. For each parametric combination of the WAAM process parameters, a sample of length 75 mm was extracted to characterize the hardness as shown in Table. 4. To characterize the relationship between hardness and the length of the sample, 15 indentations were performed at 5 mm spacing between each indentation. The indentations were performed using a 500 gf (HV0.5) diamond head held for 15 s. To ensure the consistency of the data observed, another set of 15 indents was performed at 5 mm from the first one. All indents were measured with the ZWICK/ROELL ZHμ software using a 40× magnification lens.

2.7 Surrogate Modeling. Surrogate models are analytical models that can replicate the relationship between input parameters and output characteristics in a complex system. Development of surrogate models requires carrying out scientifically constructed experimental tests informed by methodically created training matrices referred to as sampling points. Surrogate models can thus be seen as a set of equations that reveals the relationship that exists between a range of targeted input and output parameters [52]. Such models have been developed for various AM techniques and applications [38,53].

The experimental trials were conducted in accordance with the training matrix, and regression analysis was employed to establish the correlation between the WAAM process variables and the resultant responses of the printed 316LSi samples. The two process variables selected as input parameters for the surrogate modeling were the wire feed speed and torch speed. Subsequently, best-fit empirical models were derived through randomized experimental data measured for the responses E , ϵ_f , σ_y , σ_{ult} , HV0.5, and D_a . The models generated were employed to determine the significance of the contributing WAAM process parameters on the characteristics of the printed 316LSi samples. By utilizing the surrogate model, it became possible to determine the optimal WAAM process parameters combination, which results in improved mechanical properties.

3 Results and Discussion

3.1 Morphology and Accuracy of the Printed Sample. Altogether nine WAAM samples were fabricated according to the different combinations of WFS and TS leading to different energy inputs (e_i). The effect of the process parameters on the ultimate

morphology of the printed samples is illustrated in Fig. 4. It can be seen that a lower WFS results in a cleaner part (Figs. 4(a), 4(d), and 4(g)) with fewer geometrical defects at the global scale. Thanks to a lower heat input induced by a lower WFS less geometrical defects occur [54]. Moreover, once layers are being built on top of one another, side collapse may appear due to excessive heat at the beginning of layers [8]. The printed tracks are also thinner which results in a final part closer to the original ideal geometry informed by CAD. The main geometrical defects at the global scale are primarily influenced by the high energy input signified by spattering and edge collapsing as shown in Figs. 4(b), 4(c), and 4(e). Spattering, melt pool overflowing, and edge collapsing are due to the instability of the process and result in a poorer surface finish around the edges [8].

Although these are evident in Figs. 4(f), 4(h), and 4(i) to a smaller extent, the phenomenon is particularly obvious in Figs. 4(b), 4(c), and 4(e). Edge collapsing in additive manufacturing is primarily due to excessive heat when depositing a new layer over the previous one [55]. This phenomenon can be perceived as an arc shape that is magnified by the number of layers, causing a variation in the overall height between the edges and the center. This is particularly visible in the parts corresponding to Figs. 4(b), 4(c), and 4(e).

Figure 5 shows the scanned data of all the WAAM samples with the deviation from the ideal geometry highlighted. The color scale highlights the zone of minimum and maximum deviation from the ideal.

Comparing the data, it is clear that the sample shown in Fig. 5(d) shows the minimum deviation offering the best dimensional accuracy of all the samples fabricated. The worst dimensional accuracy was observed for the sample presented in Fig. 5(c) showing significant spattering, and edge collapse leading to an arch shape. The reasons for this can be explained by looking at the effect of torch speed and wire speed through the heat input (Eq. (1)) on the dimensional accuracy as shown in Figs. 6(a) and 6(b).

The reason for the variation in dimensional accuracy (D_a) between the WAAM printed samples is evident from Fig. 6(a). The data show that the lowest cloud-to-cloud distance, thus the highest dimensional accuracy, is when the heat input is low. This shows that a low heat input, driven by a high TS and a low WFS, results in a more precise geometry of the printed part. On the other hand, parts printed at high energy input, with higher WFS, present a poorer geometrical accuracy.

Figures 6(a) and 6(b) demonstrate that the fluctuation in the mean and maximum distance, which is influenced by the energy input of the WAAM process, falls within the range of 0.63–2.93 mm and 9.10–22.06 mm, respectively. Translating this to design guidelines suggests that the WAAM process can lead to a deviation of 0.35% in dimensional accuracy when using a wire diameter of 1.2 mm. For both mean and maximum deviation, the worst and best correspond to the higher and lower energy input, respectively. Overall, Figs. 6(a) and 6(b) show that a linear relationship ($R^2 = 0.8287$) and ($R^2 = 0.6233$) exists between e_i and the dimensional accuracy for the parts being analyzed. This means that an optimum WAAM process parametric should feature a WFS and TS combination leading to a low energy input that is sufficient for creating a consistent melt pool. Further analysis of the interdependency on the process parameters is carried out using the surrogate model later in this article.

3.2 Mechanical Properties

3.2.1 Tensile Properties. The stress–strain (σ – ϵ) data extracted from experimental tests carried out on all WAAM specimens informed by the training matrix at different energy inputs are shown in Fig. 7. The σ – ϵ data are further collated based on the sample build orientation where Figs. 7(a) and 7(b) show the performance of the vertical (V) and horizontal (H) samples, respectively. The curves are representative of the standard stress–strain response

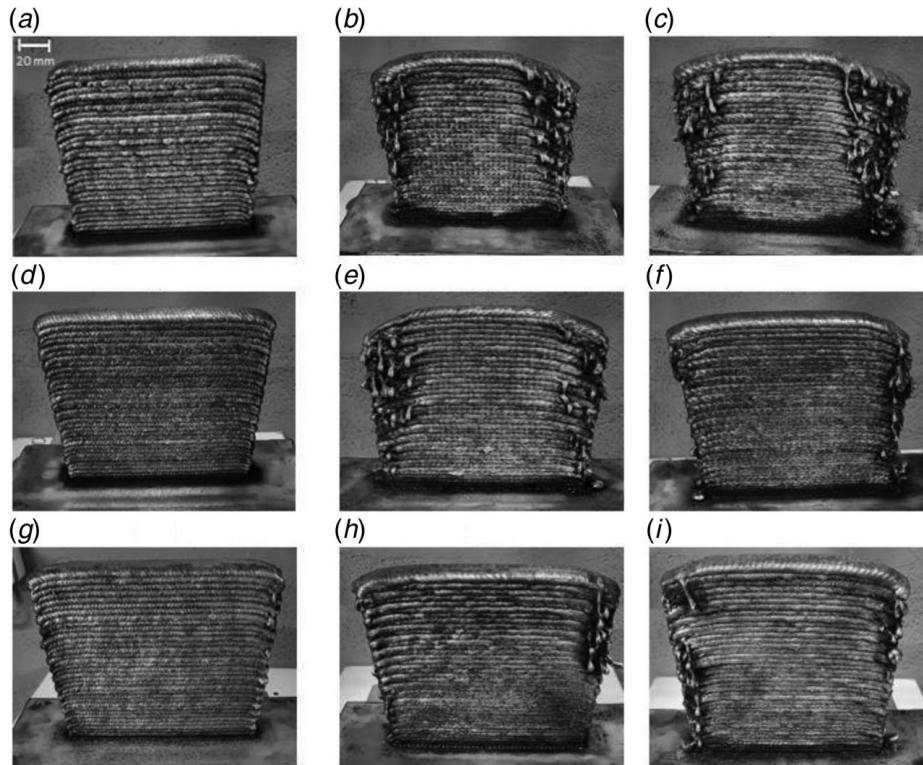


Fig. 4 Images of the additively produced components, fabricated using randomized combinations of process parameters (where WFS represents the wire feed speed, and TS represents the torch speed) that were later employed to train the surrogate model, as specified in Table 1

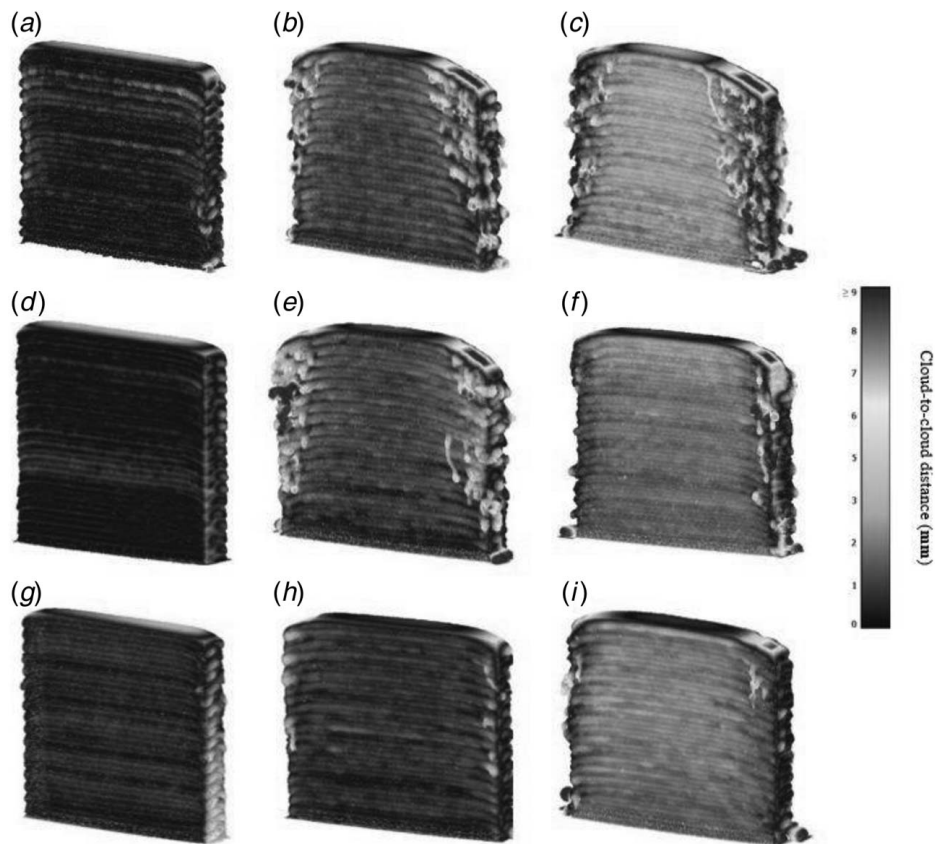


Fig. 5 Points cloud comparison between ideal geometry and additively manufactured 316LSi featuring the process parameters detailed in Table 1

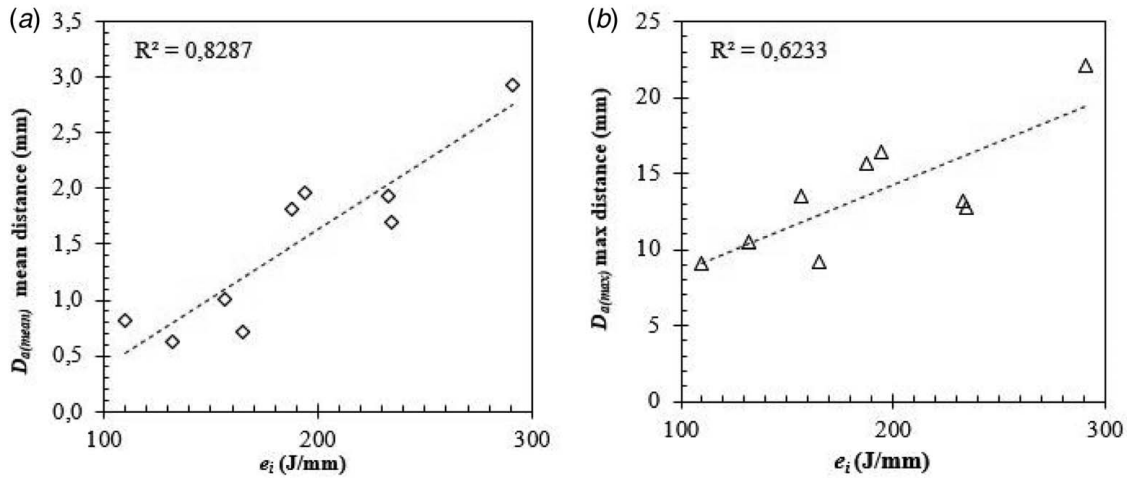


Fig. 6 Dimensional accuracy of the printed samples in comparison to ideal geometry as a function of heat input showing (a) the mean and (b) the maximum cloud-to-cloud distance between the manufactured 316LSi samples and the ideal geometry

expected from bulk metals with no spurious effects confirming that any differences observed are informed by the WAAM process.

Comparing the data between vertical (Fig. 7(a)) and horizontal (Fig. 7(b)) build orientation, no significant differences were observed at similar energy input indicating an isotropic behavior of the printed samples. This means that for the cold metal transfer WAAM process, austenitic stainless steel 316LSi can be printed either in vertical or horizontal orientation without any difference in the mechanical properties if the energy input is within 110–291 J/mm. In comparison studies conducted by Müller et al. [56], Sun et al. [57] and Cunningham et al. [28] reported the potential for anisotropy when printing steel using WAAM. In general, the variation in mechanical properties among different printing directions is attributed to interlayer softening caused by an inhomogeneous microstructure, as well as non-uniform strain distribution resulting from differential cooling. However, the findings here seem to suggest that the tendency for anisotropy is insignificant when printing thicker parts, especially at lower energy inputs (110–216 J/mm). This might be mainly influenced here by the interlayer temperature set at 400 °C and by the heat treatment applied to all printed parts. Nevertheless, the elastic modulus (105–156 GPa) dictating the material stiffness is consistent with the WAAM of thinner samples as reported in the literature [28].

Looking at the yield and ultimate strength, the data indicate that the WAAM samples are performing in the range of 281–314 MPa and 572–603 MPa, respectively, which are higher than the industry requirement. The observations are also consistent with the literature on thin samples printed at or higher energy inputs. Comparing the data based on energy input indicates that irrespective of the print orientation used, the mechanical performance of the printed samples is significantly influenced by e_i . Looking at the deviation rate, the highest difference was observed for elastic modulus which is consistent with the literature at a difference of 33% between lower and higher values [28]. The lowest influence of e_i was found for σ_{ult} indicating a 5% difference between the extremities. When it comes to failure strain which signifies the elastic and plastic elongation, a difference of 14% was observed as a result of varying the energy input. Overall, the relationship between the mechanical properties (E , ϵ_f , σ_y and σ_{ult}) of the WAAM samples and the energy input depend upon the wire speed and torch speed. These aspects are explored and mathematically quantified using the surrogate model later in the analysis.

Analyzing the failure strain for WAAM 316LSi as shown in Fig. 7, the strain associated with failure is representative of a ductile metallic material. The ductile classification is appropriate as the failure strain exceeds 38% strain at fracture for all the process parameter combinations tested. The most ductile behavior signified by a 44% ϵ_f was

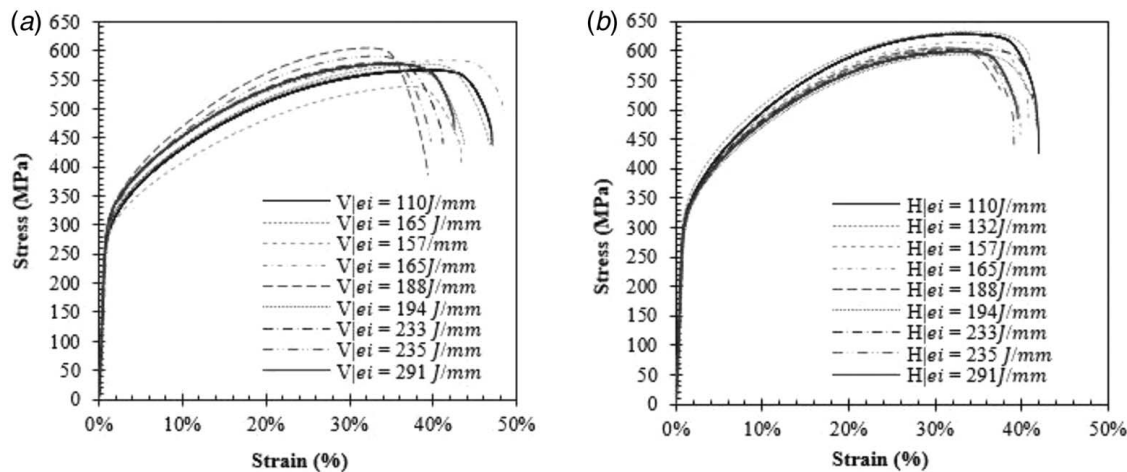


Fig. 7 Stress–strain curves of WAAM parts sorted by energy input and direction of the tensile specimen showing (a) vertical samples and (b) horizontal samples

Table 5 Comparison of mechanical characteristics of 316LSi stainless steel material manufactured from different techniques

Process	σ_{ult} (MPa)	σ_y (MPa)	E (GPa)	ϵ_f	Ref.
Cast	552	262	–	40%	[58]
Wrought	525–623	255–310	–	30%	[59]
Industry-standard	450	170	190	40%	[32]
WAAM	533 ± 23	235 ± 6	–	48 ± 2%	[32]
WAAM	550 ± 6	418	–	–	[31]
WAAM	549–582	297–330	112–192	35–47%	[28]
WAAM CMT	572–603	281–314	105–156	38–44%	Present study

revealed by two samples printed at 110 and 132 J/mm that correspond to the two lowest energy inputs used. The amount of plastic strain quantified by ϵ_f becomes important when using steel for fabricating energy absorption structures. For these applications, materials with high ductility offer higher performances as they can sustain larger plastic deformation. In this regard, fabrication techniques that can preserve or enhance high ϵ_f of materials are significant. In this regard, WAAM seem to offer a wide range of ϵ_f customizability depending on the energy input.

The mean values of experimentally obtained E , ϵ_f , σ_y , and σ_{ult} from 316LSi WAAM samples are compared with typical values observed from conventionally fabricated samples as listed in Table 5.

It can be seen that yield and ultimate strength of WAAM-fabricated 316LSi significantly outperform conventional fabricated samples. The elastic modulus data of WAAM 316LSi samples are rare in the literature; however, comparison with industry requirements for 316LSi suggests that the WAAM samples are underperforming by 19.65%. Nevertheless, ϵ_f , σ_y , and σ_{ult} obtained are consistent with the requirements of the industry. These trends indicate the importance of multi-objective optimization and surrogate modeling of the WAAM process parameters to print components with targeted performance requirements.

3.2.2 Hardness. Analysis of the data as shown in Fig. 8(a) shows a complex relationship between the wire and torch speed of the WAAM process concerning the hardness of printed 316LSi. At lower WFS of 5 m/min, the hardness seems to vary by 4.2% at a TS range of 0.6–0.9 m/min. This trend seems to be consistent also at high WFS of 10 m/min resulting in a hardness variation of 4.5%. However, when a medium WFS of 7.5 m/min was used, the influence of TS seems to be significant leading to only a 0.7% variation in the hardness data measured. The hardness of the printed samples varied between 195 and 209 HV0.5 with no significant correlation to the energy input as shown in Fig. 8(b). These

findings are consistent with the observations of Bourlet et al. [3] in another grade of stainless steel manufactured by WAAM. Although the mean hardness values observed are consistent with the literature [31,32], no influence of sample or print height on the data was observed.

3.3 Surrogate Modeling

3.3.1 Training Matrix and Regression Analysis. The analysis thus far establishes the need for effective control of WAAM process parameters namely wire and torch speed for targeted mechanical properties. Doing this on a case-by-case basis requires establishing accurate analytical relationships between the parameters (WFS and TS) and responses (E , ϵ_f , σ_y , σ_{ult} , D_a , and HV0.5) of interest. To establish the relationship between the process and properties, a randomized central composite design training matrix was developed, which is presented in Table 6.

Keeping all the other parameters constant, two WAAM process parameters (WFS and TS) that have the highest influence on the heat input were chosen as the variable factors. Informed by the parametric combinations of the matrix, samples were printed using 316LSi stainless steel. These samples were subsequently characterized for their mechanical properties as listed in Table 5 which acts as the basis for the surrogate model. After performing regression analysis on the training data in Table 5 and utilizing the best-fit indicators, it was found that the ultimate tensile strength, yield strength, elastic modulus, and fracture strain have a quadratic relationship with the WAAM process parameters, as shown in Eqs. (5)–(8). A quadratic relationship usually signifies significant interaction effects among the considered process parameters. The presence of interaction effects indicates the need for a critical understanding of both individual and cumulative contributions of the selected process variables to accurately control the properties of the printed samples. When it comes to dimensional accuracy, a two-factor interaction model with the process parameters as shown in

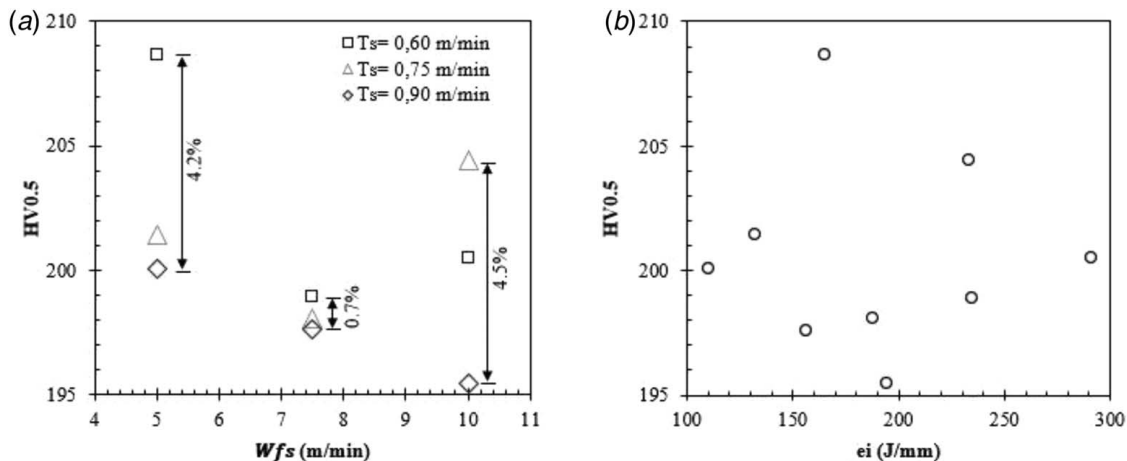


Fig. 8 Vickers hardness measurements at 500 gf for 15 s on wire arc additively manufactured 316LSi samples showing the influence of (a) WFS and TS and (b) heat input

Table 6 The surrogate model training matrix indicates the randomized parameters and the corresponding measured responses

Variable factors		Responses					
A = WFS (m/min)	B = TS (m/min)	σ_{ult} (MPa)	σ_y (MPa)	E (GPa)	ϵ_f	HV0.5	D_a
7.50	0.75	603	296	105	38%	198	98.87%
7.50	0.90	572	286	118	41%	198	99.37%
7.50	0.75	603	296	105	38%	198	98.87%
7.50	0.75	603	296	105	38%	198	98.87%
7.50	0.75	603	296	105	38%	198	98.87%
5.00	0.90	584	281	141	44%	200	99.49%
5.00	0.75	602	299	146	44%	201	99.61%
5.00	0.60	602	299	156	43%	209	99.55%
7.50	0.60	597	295	132	40%	199	98.39%
10.00	0.90	577	301	139	43%	195	98.77%
10.00	0.75	592	314	154	41%	204	98.80%
10.00	0.60	591	300	134	42%	201	98.17%

Note. WFS represents the wire feed speed, and TS is the torch speed. The responses measured include σ_{ult} (ultimate tensile strength), σ_y (yield strength), E (elastic modulus), ϵ_f (fracture strain), HV0.5 (Vickers hardness), and D_a (dimensional accuracy).

Eq. (9) has been identified. The regression analysis on hardness data indicated a random response, meaning any relationship is not directly linked to WFS and TS.

$$\sigma_{ult} = 329 - 1.7WFS + 826TS + 3.3WFS \cdot TS - 0.17WFS^2 - 609TS^2 \quad (5)$$

$$\sigma_y = 230 - 25.3WFS + 438TS + 12.6WFS \cdot TS + 1.22WFS^2 - 375TS^2 \quad (6)$$

$$E = 669 - 88WFS - 577TS + 13.8WFS \cdot TS + 5.1WFS^2 + 297TS^2 \quad (7)$$

$$\epsilon_f = 1.07 - 0.08WFS - 1.01TS + \frac{2.9}{1000}WFS \cdot TS + \frac{5.2}{1000}WFS^2 + 0.68TS^2 \quad (8)$$

$$D_a = 1.02 - \frac{5.3}{1000}WFS + 0.02TS + \frac{4.4}{1000}WFS \cdot TS \quad (9)$$

3.3.2 Model Accuracy. Table 7 summarizes the results of the analysis of variance used to evaluate the accuracy of the surrogate models developed. The relevant accuracy indicators, including the probability (p -value), coefficient of determination (R^2), adjusted R^2 , and adequate precision, were considered. The F -values were high, and the p -values were very low for all models, indicating their significance. According to statistical standards, surrogate models with a p -value of less than 0.05 and an adequate precision ratio greater than four indicate an accurate model [60]. Furthermore, the R^2 and adj- R^2 values approaching one also confirm that the surrogate models are accurate for all the considered responses.

Figure 9 illustrates the correlation between the genuine responses and the ones obtained from the surrogate model.

The actual values measured from the experiments seem to closely match the predictions indicating the validity of the surrogate model. Looking at the residuals (difference between predicted and actual value) and considering a worst-case scenario, the models offer an accuracy of 99%, 98.9%, 88.9%, 97.2%, and 99.7% for σ_{ult} , σ_y , E , ϵ_f , and D_a , respectively. However, for most predictions other than for the worst-case, the accuracy should be much higher than those mentioned. In general, the results of the analysis of variance indicate that the models created in this research are appropriate for generating accurate forecasts. As a result, Eqs. (2)–(6) effectively depict the association between the wire feed speed, torch speed, the resulting mechanical properties, and the dimensional accuracy of WAAM 316LSi.

3.3.3 Influence of Wire Feed Speed. The influence of WFS on the mechanical properties and dimensional accuracy of WAAM-fabricated 316LSi steel at a constant TS of 0.75 m/min is shown in Fig. 10.

Looking at the ultimate tensile strength of the printed steel as shown in Fig. 10(a), an almost linear trend to WFS can be observed. The highest σ_{ult} of 605 MPa was observed at the lowest WFS of 5 m/min and then decreasing linearly to 596 MPa as the WFS increased to 10 m/min. This indicates that controlling the WFS can influence the σ_{ult} of WAAM 316LSi by 1.5%. In comparison, the yield strength (Fig. 10(b)) seems to show a quadratic relationship to wire feed speed. Here, the critical WFS seems to be 7.5 m/min after which the σ_y rises consistently with subsequent increases in WFS reaching a peak of 310.5 MPa which is an improvement of 4.9%. However, changes in WFS speed below the critical speed of 7.5 m/min did not seem to significantly affect the yield strength of the printed material.

Table 7 The statistical technique called analysis of variance demonstrating the precision of the surrogate model

Model	F -value	p -Value	Statistical measurements		
			R^2	Adj- R^2	Adeq-precision
σ_{ult} (MPa)	21.68	0.0004	0.9393	0.8960	13.1569
σ_y (MPa)	36.21	<0.0001	0.9628	0.9362	22.4262
E (GPa)	8.44	0.0071	0.8578	0.7562	7.4963
ϵ_f (%)	25.02	0.0002	0.9470	0.9092	12.9107
D_a (%)	20.55	0.0002	0.8301	0.7721	14.2207

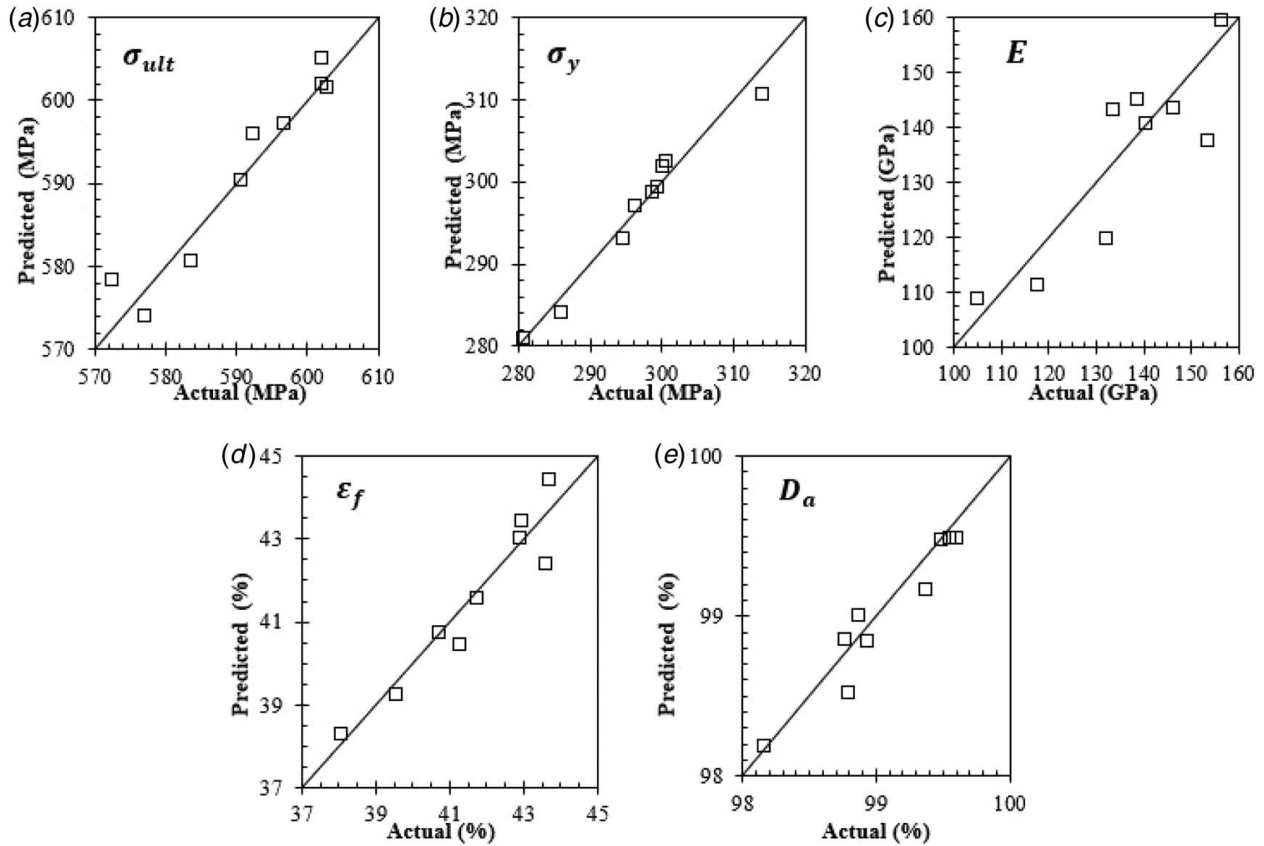


Fig. 9 The precision of the surrogate model is exhibited through a comparison of the forecasted and experimentally measured values for the parametrically produced 316LSi parts for (a) σ_{ult} , (b) σ_y , (c) E , (d) ϵ_f , and (e) D_a

The elasticity modulus and fracture strain showed a comparable quadratic relationship when it comes to the influence of WFS as shown in Figs. 10(c) and 10(d). For both cases, the lowest performance of 108.5 GPa and 38% for E and ϵ_f , respectively, was observed around a WFS of 7.5 m/min. Any reduction or increase in wire feed speed from this mid-point seems to increase both the stiffness and ductility of the printed steel. However, in both cases, the highest performance seems to be when WFS is at its lowest offering a 27.4% and 10% improvement in E and ϵ_f , respectively. Characterizing the influence of WFS on the dimensional accuracy of the printed samples reveals a linear relationship as shown in Fig. 10(e). The inverse relationship means that the higher the wire feed speed, the less accurate is the part geometry in comparison to ideal CAD. Overall, the parametric analysis indicates that the use of low WFS is beneficial for improving σ_{ult} , E , ϵ_f , and D_a . However, improving the yield strength requires the use of higher WFS around 10 m/min which suggests that the mechanical performance is influenced by the interaction effects of the process parameters which are considered in subsequent sections.

3.3.4 Influence of Torch Speed. The effect of TS on the mechanical characteristics and the dimensional accuracy of the printed material is shown in Fig. 11 for a constant WFS of 7.5 m/min.

The ultimate tensile strength (Fig. 11(a)) and the yield strength (Fig. 11(b)) of the WAAM 316LSi stainless steel demonstrate a concave quadratic relationship to torch speed. The highest σ_{ult} of 603 MPa was observed at a torch speed of 0.7 m/min which is neither the highest nor the lowest TS being tested. Increasing WFS further seems to gradually decrease the σ_{ult} to the lowest performance of 579 MPa at the highest TS of 0.9 m/min. Looking at the yield strength, a similar trend can be observed with a highest of 297.5 MPa at a TS of 0.7 m/min which subsequently decreased

to 284 MPa as TS increased to 0.9 m/min. Therefore, it is clear that σ_{ult} and σ_y of the 316LSi WAAM material are varying at 4% and 4.5% as a result of torch speed.

In comparison, the elastic modulus (Fig. 11(c)) and the failure strain (Fig. 11(d)) show a convex quadratic relationship to TS. This indicates that the elastic modulus peaked (119.5 MPa) at a torch speed of 0.6 m/min before decreasing to 108 MPa as TS was lowered to 0.8 m/min. This resulted in an overall variation of 10% in elastic modulus at a torch speed range of 0.6–0.9 m/min. For ϵ_f , the lowest ductility of 38.2% elongation was at a torch speed of 0.72 m/min before increasing to 40.4% at 0.9 m/min, which is an improvement of 5.6%. Characterizing the influence of TS on the dimensional accuracy of the printed samples reveals a linear relationship as shown in Fig. 11(e). This suggests that the dimensional accuracy improved consistently as TS was increased leading to the most accurate prints at the highest TS of 0.9 m/min. This means that parts with higher dimensional accuracy are fabricated at higher TS values. This trend is consistent with the performance of ϵ_f also offering improved ductility at high TS. Nevertheless, this observation does not translate to the mechanical strength of the printed samples as high torch speed leads to lower yield and ultimate strengths. The analysis shows that the mechanical strength parameters at a torch speed of 0.7 m/min outperformed all other parametric values for σ_{ult} and σ_y . This induces the investigation of interaction effects of the process parameters which influence the mechanical performance as explained in subsequent sections.

3.3.5 Interactions Effects of the Wire Feed Speed and Torch Speed. Although WFS and TS can be varied independently, the analysis so far confirms that their interaction has the most significant effect on the material properties and the accuracy of the printed samples. This is not surprising as these two WAAM

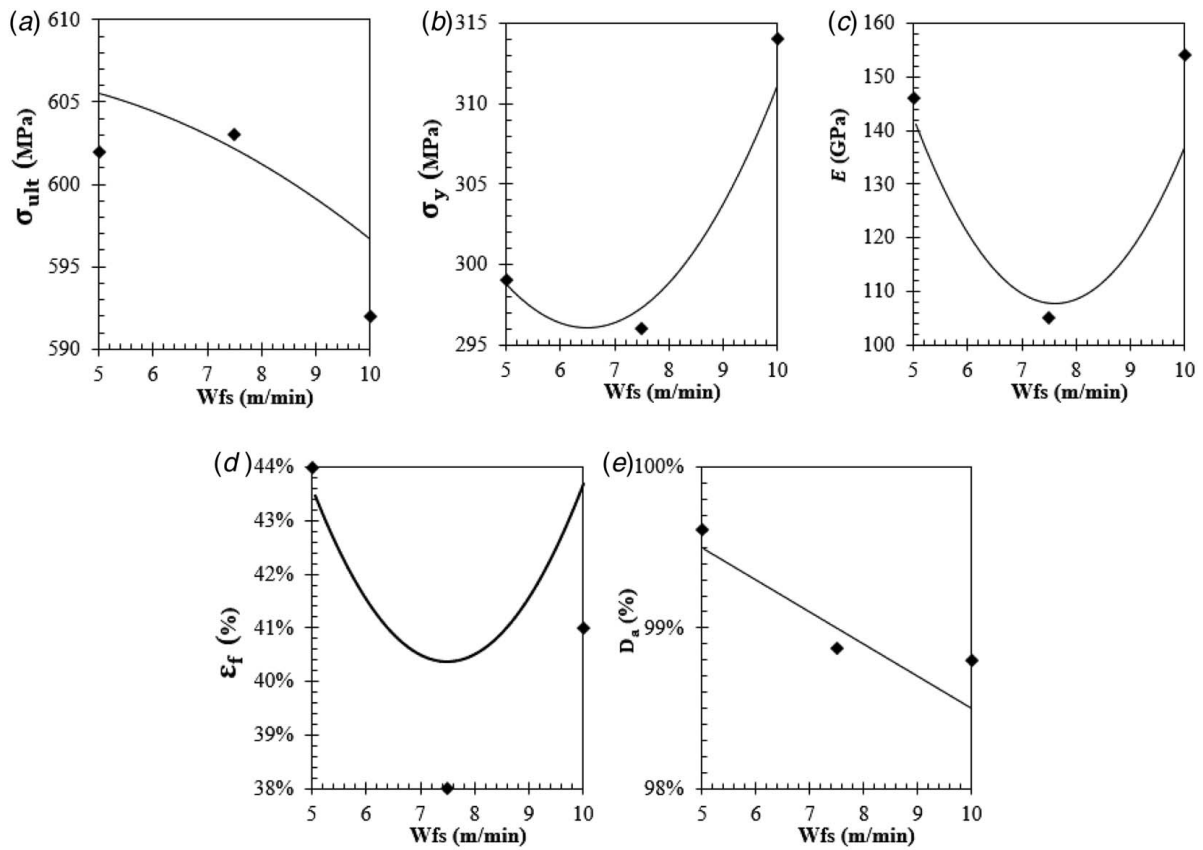


Fig. 10 Influence of wire feed speed on (a) σ_{ult} , (b) σ_y , (c) E , (d) ϵ_f , and (e) D_a with experimental points

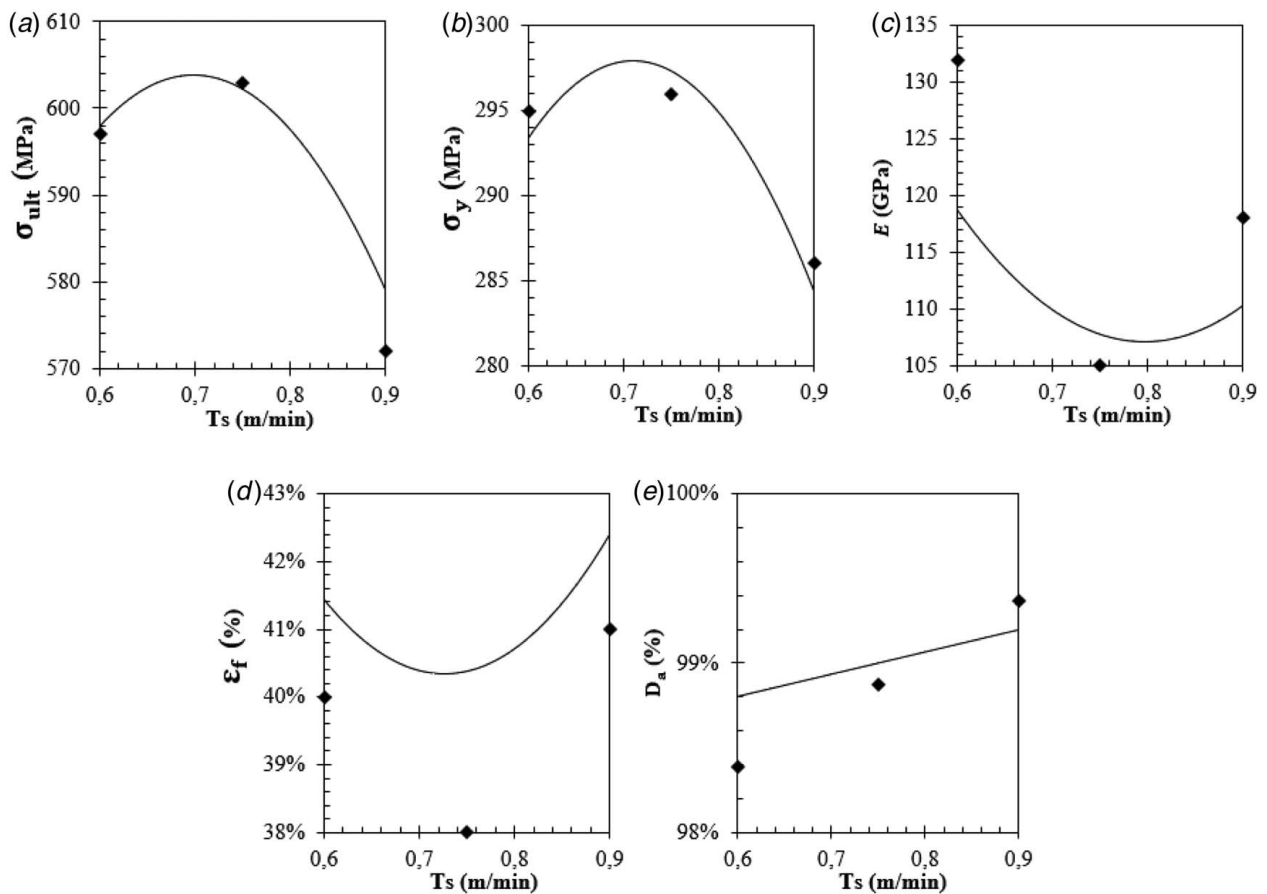


Fig. 11 Influence of torch speed on (a) σ_{ult} , (b) σ_y , (c) E , (d) ϵ_f , and (e) D_a with experimental points

process parameters are directly related to informing the energy input during the printing process. As such, studying the interaction effects between these two process parameters and identifying their order of influence are critical in evaluating their cumulative influence on the material properties. The interaction effects of WFS and TS on all the performance parameters of the printed 316LSi steel are shown in Fig. 12.

Looking at the ultimate tensile strength of the printed steel as shown in Fig. 12(a) reveals the interdependence of process parameters with TS having a higher significance to WFS. The peak ultimate strength can be observed as a cumulative effect of TS and WFS being at 0.73 m/min and 5.6 m/min, respectively. Overall, the most significant terms on σ_{ult} are the second-order and first-order effects of TS and WFS followed by their interaction effects in the order $TS^2 > TS > WFS > WFS \cdot TS > WFS^2$. This means that if the goal is to achieve the highest ultimate tensile strength for the printed materials, interaction effects between the torch speed and wire speed have to be considered in identifying the optimum process parameters.

The yield strength of the printed material as shown in Fig. 12(b) reveal significant interdependencies between WFS and TS. The highest yield strength of 311 MPa was observed because of the cumulative effect of torch and wire feed speed of 0.75 m/min and 10 m/min, respectively. Overall, the most significant terms on σ_y are the first- and second-order effects of wire feed speed and torch speed followed by their interaction effects in the order $WFS > TS^2 > WFS^2 > TS > WFS \cdot TS$. As all terms of the model are significant, optimizing WFS and TS is critical in achieving the desired yield strength when WAAM processing 316LSi.

Figure 12(c) shows the interaction effects of the WAAM process parameters on the elastic modulus of the printed material. Although there exists an interaction between both the process parameters, the data reveal WFS as having a higher influence in dictating E in comparison to TS. As such the most significant term is the second-order effect of the wire speed in the order

$WFS^2 > TS^2 > TS > WFS \cdot TS > WFS$. This means that if the target is to obtain a stiffer material with maximum elastic modulus, a combination of low TS and WFS around 0.6 m/min and 5 m/min, respectively, are warranted.

Other than stiffness and strength, ductility is a critical parameter when it comes to additively manufactured materials. As such the analysis of the interaction effects is extended to characterizing the failure strain where a higher failure strain indicates an improved ductility. Analyzing the data shown in Fig. 12(d) indicates that both WFS and TS are significant when it comes to the failure strain of the material. It appears that the fabricated material is more ductile when the torch speed and wire feed speed are around the extremities. This means that good ductility can be achieved in WAAM printed 316LSi when both WFS and TS are either low or high. For the process parameter ranges considered in this study, peak ϵ_f was observed at a combination of 5 m/min (WFS) and 0.87 m/min (TS). Overall, the most significant terms on ϵ_f are the second-order effects of wire feed speed and torch speed followed by their first-order effects and the interaction effects in the order $TS^2 > WFS^2 > TS > WFS > WFS \cdot TS$. Consequently, optimizing the elongation of the WAAM 316LSi requires careful consideration of both TS and WFS.

Lastly, the influence of the process parameter interaction on the dimensional accuracy is shown in Fig. 12(e). The interaction effect is only significant at high WFS of around 10 m/min. As such for much of the process parameter ranges considered in this study, both WFS and TS seem to be influencing the parts independently in a linear fashion. However, TS has a higher significance in dictating the dimensional accuracy of the parts in comparison to WFS. Overall, the most significant terms on D_a are the first-order effects of wire feed speed and torch speed followed by their interaction effects in the order $WFS > TS > WFS \cdot TS$. Therefore, to achieve high dimensional accuracy for WAAM printed steel, interaction effects between the wire feed speed and the torch speed must be considered although to a relatively lesser extent. Considering all

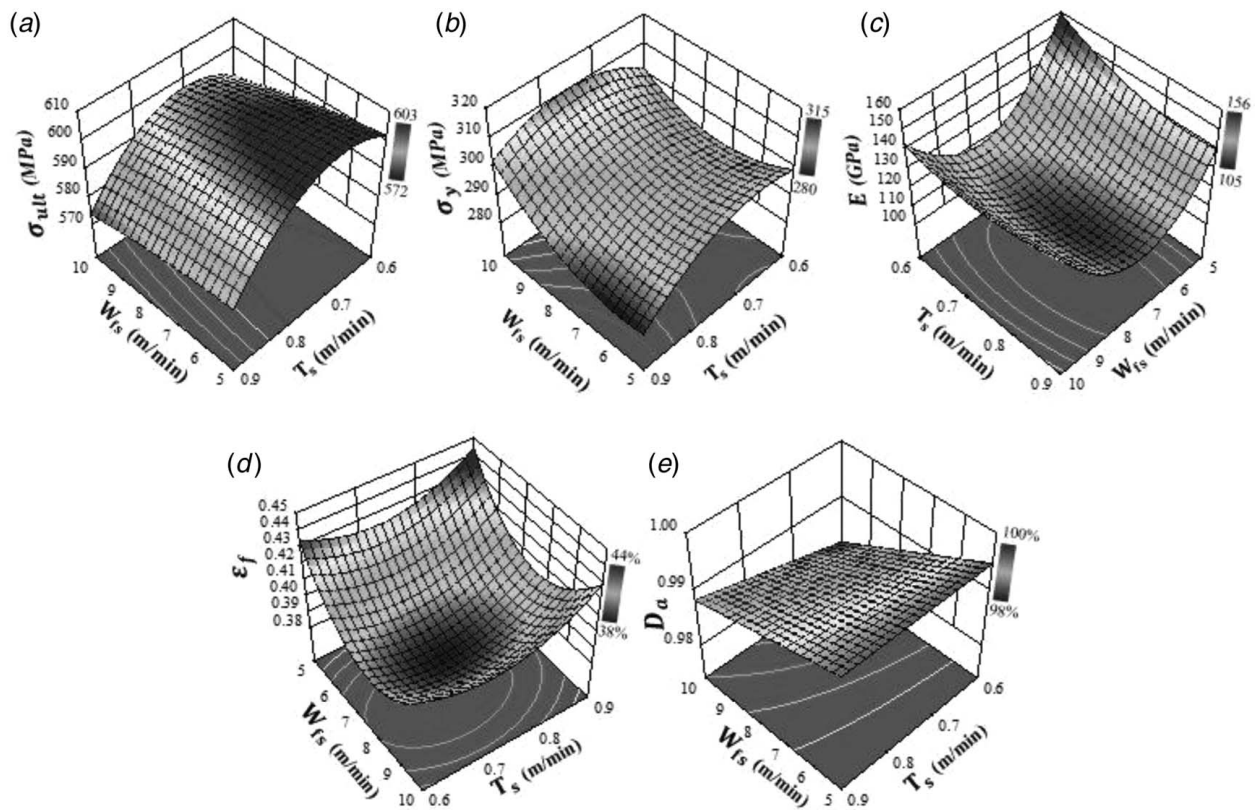


Fig. 12 Influence of process parameters on WAAM 316LSi showing interaction effects between wire feed speed and torch speed on (a) σ_{ult} , (b) σ_y , (c) E , (d) ϵ_f , and (e) D_a

Table 8 Synthesis of the optimum values from the surrogate model for the mechanical properties considered according to the range of tested WFS and TS

Mechanical properties	Optimum value	Corresponding WFS (m/min)	Corresponding TS (m/min)
σ_{ult} (MPa)	606	5.6	0.73
σ_y (MPa)	311	10	0.75
E (GPa)	157	5.0	0.61
ϵ_f (%)	44	5.0	0.87
D_a (%)	99.6	5.0	0.6

the analyses, the optimum values from the surrogate modeling for the mechanical properties of WAAM printed steel are summarized in Table 8. These data show the potential of using WAAM in an industrial setting depending upon the dimensional accuracy and properties required.

4 Conclusion

The mechanical properties of WAAM-processed metals are of significant interest to the industrial community. Despite this, comprehensive models that can predict the influence of relevant process parameters on the resulting properties of 316LSi steel are yet to be reported. As such, the paper reveals the first surrogate model that can predict the influence of wire and torch speed on both the mechanical properties and dimensional accuracy of WAAM-processed 316LSi steel. The surrogate model was informed by experimentally conceived training data that found an isotropic behavior of WAAM printed steel for thick parts (25 mm—0.98 in.). It was also found that carefully controlling the wire and torch speed can lead to ultimate tensile strength (606 MPa), yield strength (311 MPa), and failure strain (44%) that meets or exceeds the industry requirement for 316LSi steel. While the mean hardness (202 HV0.5) of the printed samples was consistent with the literature, no variation according to print height was observed. When it comes to the quality of the printed samples, a low wire feed speed of 5 m/min (39.4 in./min) was found to print samples at an accuracy of 99.6% in comparison to the ideal CAD. The elastic modulus of the printed samples was found to be in the range of 105–157 GPa depending upon the parametric combination of wire and torch speeds used allowing stiffness personalization. The surrogate model found that the ductility of the printed steel was primarily influenced by wire feed speed and can offer up to 44% elongation. The study found significant interaction effects between different WAAM process parameters for all mechanical properties. The TS was found to be more significant in comparison to WFS for ultimate tensile strength (σ_{ult}) and failure strain (ϵ_f). On the contrary, the yield strength (σ_y), elastic modulus (E), and dimensional accuracy (D_a) were found to be primarily driven by wire feed speed as opposed to torch speed. The proposed surrogate model drastically reduces the pre-processing requirements of WAAM printed 316LSi steel and allows the manufacturer to control the process to obtain targeted mechanical properties.

Acknowledgment

The findings of this research project are a result of collaborative research between ESTIA and the Additive Manufacturing of Functional Materials (AMFM) research group from the University of Wolverhampton. It was technically supported by ADDIMADOUR, Additive Manufacturing Solutions, a platform from ESTIA.

Author Contribution

The study's conception and design were a collaborative effort by all authors. Laurent Terrenoir, Julie Lartigau, and Arun Arjunan

conducted the material preparation, data collection, and analysis. Laurent Terrenoir initially drafted the manuscript, which was subsequently reviewed and edited by all authors. The final manuscript was read and approved by all authors.

Funding Data

This research project was undertaken with the funding of University of Bordeaux and Communauté d'Agglomération Pays Basque (CAPB).

Conflict of Interest

There are no conflicts of interest.

Data Availability Statement

The authors attest that all data for this study are included in the paper.

Nomenclature

- E = elastic modulus
- e_i = calculated energy input or heat input of the WAAM process
- D_a = dimensional accuracy as defined in Eq. (4)
- $D_{a(max)}$ = maximum dimensional accuracy refers to the maximum cloud to cloud distance measured for a specific part
- $D_{a(mean)}$ = mean dimensional accuracy refers to the mean cloud to cloud distance measured for all points of each part
- AM = additive manufacturing
- CAD = computer-aided design
- HV0.5 = Vickers hardness measured at 500 gf
- TS = torch speed
- WAAM = wire arc additive manufacturing
- WFS = wire feed speed
- ϵ_f = failure strain
- σ_{ult} = ultimate tensile strength
- σ_y = yield strength
- 316LSi = stainless steel 316L

References

- [1] ISO/ASTM 52900:2021(E), 2021, "Additive Manufacturing—General Principles—Fundamentals and Vocabulary, International Organization for Standardization," <https://www.iso.org/obp/ui/#iso:std:iso-astm:52900:ed-2:v1:en>
- [2] Ahn, D. G., 2021, "Directed Energy Deposition (DED) Process: State of the Art," *Int. J. of Precis. Eng. and Manuf.-Green Tech.*, **8**, pp. 703–742.
- [3] Bourlet, C., Zimmer-Chevret, S., Pesci, R., Bigot, R., Robineau, A., and Scandella, F., 2020, "Microstructure and Mechanical Properties of High Strength Steel Deposits Obtained by Wire-Arc Additive Manufacturing," *J. Mater. Process. Technol.*, **285**, p. 116759.
- [4] Li, J. Z., Alkahari, M. R., Rosli, N. A. B., Hasan, R., Sudin, M. N., and Ramlil, F. R., 2019, "Review of Wire Arc Additive Manufacturing for 3d Metal Printing," *Int. J. Autom. Technol.*, **13**(3), pp. 346–353.
- [5] Bevans, B., Ramalho, A., Smoqi, Z., Gaikwad, A., Santos, T. G., Rao, P., and Oliveira, J. P., 2023, "Monitoring and Flaw Detection During Wire-Based Directed Energy Deposition Using In-Situ Acoustic Sensing and Wavelet Graph Signal Analysis," *Mater. Des.*, **225**, p. 111480.
- [6] Li, S., Li, J. Y., Jiang, Z. W., Cheng, Y., Li, Y. Z., Tang, S., Leng, J. Z., et al., 2022, "Controlling the Columnar-to-Equiaxed Transition During Directed Energy Deposition of Inconel 625," *Addit. Manuf.*, **57**, p. 102958.
- [7] Zuo, X., Zhang, W., Chen, Y., Oliveira, J. P., Zeng, Z., Li, Y., Luo, Z., and Ao, S., 2022, "Wire-Based Directed Energy Deposition of NiTiTi Shape Memory Alloys: Microstructure, Phase Transformation, Electrochemistry, X-Ray Visibility and Mechanical Properties," *Addit. Manuf.*, **59**, p. 103115.
- [8] Rodrigues, T. A., Duarte, V., Miranda, R. M., Santos, T. G., and Oliveira, J. P., 2019, "Current Status and Perspectives on Wire and Arc Additive Manufacturing (WAAM)," *Materials*, **12**(7), p. 1121.
- [9] Fang, J., Wang, K., Yang, D., and Huang, Y., 2019, "Gas Flow Status Analysis in CMT+P Additive Manufacturing Based on Texture Features of Molten Pool Images," *Optik*, **179**, pp. 385–394.

- [10] Kindermann, R. M., Roy, M. J., Morana, R., and Prangnell, P. B., 2020, "Process Response of Inconel 718 to Wire + Arc Additive Manufacturing With Cold Metal Transfer," *Mater. Des.*, **195**, p. 109031.
- [11] Ali, Y., Henckell, P., Hildebrand, J., Reimann, J., Bergmann, J. P., and Barnikol-Oettler, S., 2019, "Wire Arc Additive Manufacturing of Hot Work Tool Steel With CMT Process," *J. Mater. Process. Technol.*, **269**, pp. 109–116.
- [12] Gardner, L., Kyvelou, P., Herbert, G., and Buchanan, C., 2020, "Testing and Initial Verification of the World's First Metal 3D Printed Bridge," *J. Constr. Steel Res.*, **172**, p. 106233.
- [13] Ye, J., Kyvelou, P., Gilardi, F., Lu, H., Gilbert, M., and Gardner, L., 2021, "An End-to-End Framework for the Additive Manufacturing of Optimized Tubular Structures," *IEEE Access*, **9**, pp. 165476–165489.
- [14] Feucht, T., Lange, J., Waldschmitt, B., Schudlich, A.-K., Klein, M., and Oechsner, M., 2020, "Welding Process for the Additive Manufacturing of Cantilevered Components With the WAAM," *Adv. Struct. Mater.*, **125**, pp. 67–78.
- [15] Williams, S. W., Martina, F., Addison, A. C., Ding, J., Pardal, G., and Colegrove, P., 2016, "Wire+Arc Additive Manufacturing," *Mater. Sci. Technol.*, **32**(7), pp. 641–647.
- [16] Cunningham, C. R., Flynn, J. M., Shokrani, A., Dhokia, V., and Newman, S. T., 2018, "Invited Review Article: Strategies and Processes for High Quality Wire Arc Additive Manufacturing," *Addit. Manuf.*, **22**, pp. 672–686.
- [17] Rodrigues, T. A., Escobar, J. D., Shen, J., Duarte, V. R., Ribamar, G. G., Avila, J. A., Maawad, E., Schell, N., Santos, T. G., and Oliveira, J. P., 2021, "Effect of Heat Treatments on 316 Stainless Steel Parts Fabricated by Wire and Arc Additive Manufacturing: Microstructure and Synchrotron X-Ray Diffraction Analysis," *Addit. Manuf.*, **48**, p. 102428.
- [18] Rodrigues, T. A., Duarte, V. R., Miranda, R. M., Santos, T. G., and Oliveira, J. P., 2021, "Ultracold-Wire and Arc Additive Manufacturing (UC-WAAM)," *J. Mater. Process. Technol.*, **296**, p. 117196.
- [19] Rodrigues, T. A., Cipriano Farias, F. W., Zhang, K., Shamsolhodaei, A., Shen, J., Zhou, N., Schell, N., et al., 2022, "Wire and Arc Additive Manufacturing of 316L Stainless Steel/Inconel 625 Functionally Graded Material: Development and Characterization," *J. Mater. Res. Technol.*, **21**, pp. 237–251.
- [20] Xie, B., Xue, J., and Ren, X., 2020, "Wire Arc Deposition Additive Manufacturing and Experimental Study of 316L Stainless Steel by CMT+P Process," *Metals*, **10**, p. 1419.
- [21] Evans, S. I., Wang, J., Qin, J., He, Y., Shepherd, P., and Ding, J., 2022, "A Review of WAAM for Steel Construction—Manufacturing, Material and Geometric Properties, Design, and Future Directions," *Structures*, **44**, pp. 1506–1522.
- [22] Abe, T., and Sasahara, H., 2019, "Layer Geometry Control for the Fabrication of Lattice Structures by Wire and Arc Additive Manufacturing," *Addit. Manuf.*, **28**, pp. 639–648.
- [23] Ščetinec, A., Klobčar, D., and Bračun, D., 2021, "In-Process Path Replanning and Online Layer Height Control Through Deposition Arc Current for Gas Metal Arc Based Additive Manufacturing," *J. Manuf. Process.*, **64**, pp. 1169–1179.
- [24] Xiong, J., Zhang, Y., and Pi, Y., 2020, "Control of Deposition Height in WAAM Using Visual Inspection of Previous and Current Layers," *J. Intell. Manuf.*, **32**(32), pp. 2209–2217.
- [25] Xu, B., Tan, X., Gu, X., Ding, D., Deng, Y., Chen, Z., and Xu, J., 2019, "Shape-Driven Control of Layer Height in Robotic Wire and Arc Additive Manufacturing," *Rapid Prototyp. J.*, **25**(10), pp. 1637–1646.
- [26] Wang, Y., Xu, X., Zhao, Z., Deng, W., Han, J., Bai, L., Liang, X., and Yao, J., 2021, "Coordinated Monitoring and Control Method of Deposited Layer Width and Reinforcement in WAAM Process," *J. Manuf. Process.*, **71**, pp. 306–316.
- [27] Xia, C., Pan, Z., Zhang, S., Polden, J., Wang, L., Li, H., Xu, Y., and Chen, S., 2020, "Model Predictive Control of Layer Width in Wire Arc Additive Manufacturing," *J. Manuf. Process.*, **58**, pp. 179–186.
- [28] Cunningham, C. R., Wang, J., Dhokia, V., Shokrani, A., and Newman, S. T., 2019, "Characterisation of Austenitic 316L/316Ti Stainless Steel Produced by Wire Arc Additive Manufacturing With Interlayer Cooling," *Proceedings of the 30th Annual International Solid Freeform Fabrication Symposium*, Austin, TX, Aug. 12–14, pp. 426–439.
- [29] Kyvelou, P., Huang, C., Gardner, L., and Buchanan, C., 2021, "Structural Testing and Design of Wire Arc Additively Manufactured Square Hollow Sections," *J. Struct. Eng.*, **147**(12), p. 04021218.
- [30] Laghi, V., Palermo, M., Gasparini, G., Girelli, V. A., and Trombetti, T., 2021, "On the Influence of the Geometrical Irregularities in the Mechanical Response of Wire-and-Arc Additively Manufactured Planar Elements," *J. Constr. Steel Res.*, **178**, p. 106490.
- [31] Wang, L., Xue, J., and Wang, Q., 2019, "Correlation Between Arc Mode, Microstructure, and Mechanical Properties During Wire Arc Additive Manufacturing of 316L Stainless Steel," *Mater. Sci. Eng. A*, **751**, pp. 183–190.
- [32] Chen, X., Li, J., Cheng, X., He, B., Wang, H., and Huang, Z., 2017, "Microstructure and Mechanical Properties of the Austenitic Stainless Steel 316L Fabricated by Gas Metal Arc Additive Manufacturing," *Mater. Sci. Eng. A*, **703**, pp. 567–577.
- [33] Palmeira Belotti, L., van Dommelen, J. A. W., Geers, M. G. D., Goulas, C., Ya, W., and Hoefnagels, J. P. M., 2022, "Microstructural Characterisation of Thick-Walled Wire Arc Additively Manufactured Stainless Steel," *J. Mater. Process. Technol.*, **299**, p. 117373.
- [34] Fuchs, C., Baier, D., Semm, T., and Zaeh, M. F., 2020, "Determining the Machining Allowance for WAAM Parts," *Prod. Eng.*, **14**(5–6), pp. 629–637.
- [35] Stucker, B., and Qu, X., 2003, "A Finish Machining Strategy for Rapid Manufactured Parts and Tools," *Rapid Prototyp. J.*, **9**(4), pp. 194–200.
- [36] Liu, J., Xu, Y., Ge, Y., Hou, S., and Chen, S., 2020, "Wire and Arc Additive Manufacturing of Metal Components: A Review of Recent Research Developments," *Int. J. Adv. Manuf. Technol.*, **111**(1–2), pp. 149–198.
- [37] Jin, W., Zhang, C., Jin, S., Tian, Y., Wellmann, D., and Liu, W., 2020, "Wire Arc Additive Manufacturing of Stainless Steels: A Review," *Appl. Sci.*, **10**(5), p. 1563.
- [38] Arjunan, A., Robinson, J., Baroutaji, A., Tuñón-Molina, A., Martí, M., and Serrano-Aroca, Á., 2021, "3D Printed Cobalt-Chromium-Molybdenum Porous Superalloy With Superior Antiviral Activity," *Int. J. Mol. Sci.*, **22**(23), p. 12721.
- [39] Lee, S. H., 2020, "Optimization of Cold Metal Transfer-Based Wire Arc Additive Manufacturing Processes Using Gaussian Process Regression," *Metals*, **10**(4), pp. 461–474.
- [40] ISO 14343:2017, 2017, "Welding Consumables—Wire Electrodes, Strip Electrodes, Wires and Rods for Arc Welding of Stainless and Heat Resisting Steels—Classification," <https://www.iso.org/standard/67727.html>
- [41] Müller, J., Grabowski, M., Müller, C., Hensel, J., Unglaub, J., Thiele, K., Kloft, H., and Dilger, K., 2019, "Design and Parameter Identification of Wire and Arc Additively Manufactured (WAAM) Steel Bars for Use in Construction," *Metals*, **9**(7), p. 725.
- [42] Singh, S., Kumar Sharma, S., and Rathod, D. W., 2021, "A Review on Process Planning Strategies and Challenges of WAAM," *Mater. Today Proc.*, **47**(19), pp. 6564–6575.
- [43] Koli, Y., Aravindan, S., and Rao, P. V., 2022, "Influence of Heat Input on the Evolution of δ -Ferrite Grain Morphology of SS308L Fabricated Using WAAM-CMT," *Mater. Charact.*, **194**, p. 112363.
- [44] Li, C., Gu, H., Wang, W., Wang, S., Ren, L., Wang, Z., Ming, Z., and Zhai, Y., 2019, "Effect of Heat Input on Formability, Microstructure, and Properties of Al-7Si-0.6Mg Alloys Deposited by CMT-WAAM Process," *Appl. Sci.*, **10**, p. 70.
- [45] Gordon, J. V., and Gary Harlow, D., 2019, "Statistical Modeling of Wire and Arc Additive Manufactured Stainless Steel 304: Microstructure and Fatigue," *Int. J. Reliab. Qual. Safety Eng.*, **26**(4), p. 1950016.
- [46] Rosli, N. A., Alkahari, M. R., Abdollah, M. F., Maidin, S., Ramli, F. R., and Herawan, S. G., 2021, "Review on Effect of Heat Input for Wire Arc Additive Manufacturing Process," *J. Mater. Res. Technol.*, **11**, pp. 2127–2145.
- [47] Xie, B., Xue, J., Ren, X., Wu, W., and Lin, Z., 2020, "A Comparative Study of the CMT+P Process on 316L Stainless Steel Additive Manufacturing," *Appl. Sci.*, **10**, p. 3284.
- [48] Nancharaiyah, T., Ranga Raju, D., and Ramachandra Raju, V., 2010, "An Experimental Investigation on Surface Quality and Dimensional Accuracy of FDM Components," *Int. J. Emerg. Technol.*, **1**, pp. 106–111. <https://www.researchgate.net/publication/267248480>
- [49] Eltes, P. E., Kiss, L., Bartos, M., Gyorgy, Z. M., Csakany, T., Bereczki, F., Lesko, V., Puhl, M., Varga, P. P., and Lazary, A., 2020, "Geometrical Accuracy Evaluation of an Affordable 3D Printing Technology for Spine Physical Models," *J. Clin. Neurosci.*, **72**, pp. 438–446.
- [50] Decker, N., Wang, Y., and Huang, Q., 2020, "Efficiently Registering Scan Point Clouds of 3D Printed Parts for Shape Accuracy Assessment and Modeling," *J. Manuf. Syst.*, **56**, pp. 587–597.
- [51] ISO 6892-1, 2019, *Metallic materials — Tensile testing — Part 1: Method of Test at Room Temperature.*
- [52] Thombre, M. N., Preisig, H. A., and Addis, M. B., 2015, "Developing Surrogate Models via Computer Based Experiments," *Comput. Aided Chem. Eng.*, **37**, pp. 641–646.
- [53] Milhomme, S., Lartigau, J., Brugger, C., and Froustey, C., 2021, "Bead Geometry Prediction Using Multiple Linear Regression Analysis: Application to Ti-6Al-4V Beads Made by Laser Metal Powder Deposition," *Int. J. Adv. Manuf. Technol.*, **117**(1–2), pp. 607–620.
- [54] Srivastava, M., Rathee, S., Tiwari, A., and Dongre, M., 2022, "Wire Arc Additive Manufacturing of Metals: A Review on Processes, Materials and Their Behaviour," *Mater. Chem. Phys.*, **294**, p. 126988.
- [55] Vo, T. H., Grandvallet, C., and Vignat, F., 2021, "A Model for Manufacturing Large Parts With WAAM Technology," *Adv. Manuf. Technol.*, **XXXIV**, pp. 1–6.
- [56] Müller, J., Hensel, J., and Dilger, K., 2022, "Mechanical Properties of Wire and Arc Additively Manufactured High-Strength Steel Structures," *Weld. World*, **66**(3), pp. 395–407.
- [57] Sun, L., Jiang, F., Huang, R., Yuan, D., Guo, C., and Wang, J., 2020, "Anisotropic Mechanical Properties and Deformation Behavior of Low-Carbon High-Strength Steel Component Fabricated by Wire and Arc Additive Manufacturing," *Mater. Sci. Eng. A*, **787**, p. 139514.
- [58] ASM International, 1980, *Metals Handbook: Properties and Selection Stainless Steels, Tool Materials and Special-Purpose Metals*, 9th ed., ASM International, Metals Park, OH.
- [59] Yadollahi, A., Shamsaei, N., Thompson, S. M., and Seely, D. W., 2015, "Effects of Process Time Interval and Heat Treatment on the Mechanical and Microstructural Properties of Direct Laser Deposited 316L Stainless Steel," *Mater. Sci. Eng. A*, **644**, pp. 171–183.
- [60] Arjunan, A., Singh, M., Baroutaji, A., and Wang, C., 2020, "Additively Manufactured AlSi10Mg Inherently Stable Thin and Thick-Walled Lattice With Negative Poisson's Ratio," *Compos. Struct.*, **247**, p. 112469.